Verification of induction zone models for wind farm annual energy production estimation

A Meyer Forsting[1], OS Rathmann[1], MP van der Laan[1], N Troldborg[1], B Gribben[2], G Hawkes[2], E Branlard[3]

[1] DTU Wind Energy, Technical University of Denmark, Roskilde, Denmark
[2] Frazer-Nash Consultancy, Dorking, UK
[3] National Renewable Energy Laboratory, Golden, USA

E-mail: alrf@dtu.dk

Abstract. Fast engineering wake models are the backbone of wind farm annual energy production (AEP) estimators, whereas the addition of induction zone models in existing tools is a more recent response to rising concerns over wind farm blockage associated losses. Here, "blockage" describes the combined induction fields of all wind turbines inside a farm. Unlike the term might suggest, blockage not only reduces flow speeds, but also increases them; for instance along the outer edges of wind farms. Evaluating the overall impact on AEP of these gains and losses necessitates accurate wind farm induction models. Whilst engineering wake models are tuned to predict wind farm performance, existing induction zone models are all derived for accurately predicting the near field induction not the far field value—important for wind farm simulations. This paper presents the induction models implemented in the wind farm simulation tool PyWake, as well as results from novel analytical models and compares their far field predictions to RANS-AD simulations of different turbines. We demonstrate that when including blockage in AEP simulations, the downstream speed-ups need to be included to avoid an unrealistic bias toward AEP loss and that wake expansion significantly impacts induction at rated thrust levels.

1. Introduction

The current industry standard treats a wind turbine in a nowadays commonly sized farm—with 50 or more rotors—as if it was standing in isolation, as long as it is not in the wake of another machine. However, over the past 5 years mounting scientific evidence is disputing the status quo and calls for considering blockage in preconstruction annual energy production (AEP) estimation. Early numerical studies at the Technical University of Denmark (DTU) [1] demonstrated that even along a single row of only five turbines-—a configuration similar to a turbine test stand-—power production could vary by up to 3% solely due to blockage. Several wind tunnel experiments with downscaled wind farms found a noticeable wind speed reduction at the most upstream, wake-free row of turbines [2]. Nygaard et al. [3] equally measured lower velocities for those turbines in their wind farms than expected for a single, isolated rotor and demonstrated with an analytical vortex model how the other downstream turbines' blockage contributed. The first attempt at quantifying the bias in the current, wakes-only AEP calculation was presented in an extensive study by Bleeg et al. [4]. Comparing wind speed measurements at locations around different wind farms before and after erection, they find significant wind

speed reduction even relatively far from the array, once the turbines went online. They quantify the bias from ignoring blockage to lie between 3-5% of the expected AEP. This is, however, a conservative estimate, as it does not consider blockage related power redistribution within the array. All studies additionally show a strong influence of the wind farm on the surrounding wind field, implying that the turbine array ultimately acts a single obstruction to the incoming flow, which diverts the flow around and above it. Increased power production at the wind farm's edges are testimony to this flow divergence. In-line with the wind farm scale, its interaction with the atmosphere is also growing. Under certain extreme conditions, computational fluid dynamics (CFD) simulations already hinted toward the possibility of wind farms inducing gravity waves above the inversion layer with grave consequences on energy production [5].

With recent research highlighting the significance of blockage in the AEP prediction, blockage models are finding their way into fast, engineering AEP estimators [3, 6]. However, none of the existing models' behaviour is verified in the far field, at a distance where they influence other turbines inside a wind farm. This paper presents six induction models implemented in the wind farm simulation tool PyWake and compares their far-field predictions to those by Reynolds-averaged Navier-Stokes actuator disc (RANS-AD) simulations of different turbines.

2. Analytical induction models

A number of induction models are implemented in DTU Wind Energy's open-source wind farm simulation tool, PyWake, capable of calculating wind farm flow fields, power production, and AEP. The vortex models have been presented before [7, 6] and were implemented following Branlard's `WIZ` [7]. We also detail some novel or otherwise relevant implementations and try to give a comprehensive overview of their theoretical foundations.

2.1. Vortex cylinder model

The vortex cylinder (VC) model prescribes the geometry of the wake to be a semi-infinite cylinder of constant tangential vorticity, γ_t, which is related to the free-stream, V_∞, and wind turbine thrust coefficient, C_T:

$$\gamma_t = -V_\infty \left[1 - \sqrt{1 - C_T}\right] = -2V_\infty a_0 \tag{1}$$

with a_0 as the axial induction factor in the rotor plane. The velocity field is obtained by integrating the Biot-Savart law (e.g., [7, 8]), such that the axial velocity perturbation is given by:

$$u(x,r) = \frac{\gamma_t}{2}\left[\frac{R - r + |R - r|}{2|R - r|} + \frac{xk(x,r)}{2\pi\sqrt{rR}}\left(K(k^2(x,r)) + \frac{R - r}{R + r}\Pi\left(k^2(0,r), k^2(x,r)\right)\right)\right] \tag{2}$$

with R denoting the rotor radius and

$$k(x,r) = \sqrt{\frac{4rR}{(R + r)^2 + x^2}} \tag{3}$$

and $K()$ and Π are the complete elliptical integrals of the first and third kind. A single vortex cylinder is used in this study, but more advanced formulations can be used to account for the distribution of thrust along the rotor span and wake rotation effect.

2.2. Vortex dipole/Rankine-half-body model

The vortex dipole (VD) model corresponds to a far-field approximation of the VC model, as the rotor vorticity is approximated by a point vortex doublet. The induced axial velocity becomes [7]:

$$u(x,r) = \frac{\gamma_t}{4}\frac{x}{r^3}R^2 \tag{4}$$

The Rankine-half-body approach proposed by Gribben and Hawkes [9], where the rotor is modelled by a potential flow point source, yields the same flow perturbations as the VD just with the addition of an equation for the stagnation line. The latter roughly encloses the wake, thus its computation is not necessary in the context of wind farm blockage.

2.3. Self-similar model

Troldborg et al. [10] derived an engineering model from the VC model and RANS simulations of different wind turbines. They found the induction zone to show radial self-similarity and—inspired by the approximate solution to the plane-jet—derived the following fit combining an axial and radial shape function:

$$u_x(x,r) = a(x)f(x,r) \tag{5}$$

$$a(x) = \frac{1}{2}\left(1-\sqrt{1-\gamma C_T}\right)\mu(x,r) \quad \text{with} \quad \mu(x,r) = \left(1+\frac{x}{\sqrt{R^2+x^2}}\right) \tag{6}$$

$$f(x,r) = \operatorname{sech}^{\alpha}\left(\frac{\beta r}{r_m(x)}\right) \quad \text{with} \quad r_m(x) = R\sqrt{\lambda\left(\eta+\frac{x^2}{R^2}\right)} \tag{7}$$

with $\gamma = 1.1$, $\beta = \sqrt{2}$, $\alpha = 8/9$, $\lambda = 0.587$, and $\eta = 1.32$. Note that the last term in the axial shape function, μ, is identical to the solution of the VC model on the rotor centre line, where $r = 0$ and the first term is identical to the expression for the axial induction in the rotor plane, except that the thrust is multiplied by γ. This coefficient had to be introduced, as the vortex cylinder consistently underestimated the axial induction with respect to the RANS results.

2.4. Rathmann model

Another recent development is the approximation by Rathmann. Similar to Troldborg et al. [10], it combines the axial VC solution with a radial shape function:

$$u(x,r) = \frac{\gamma_t}{2}\mu(x,r)G(x,r) \tag{8}$$

As in the far field ($x \ll -1$), the VC solution should tend to $\left(\frac{x^2}{x^2+r^2}\right)^{3/2}$ so should G, which also shows that G only depends on the ratio r/x. Inspecting the VC solution in the near field, suggested a close relationship between the solid angle under which the opening of the cylinder is seen from the point (x,r). The solid angle could be approximated by the "angular ellipsis" spanned by the horizontal angle 2α and the vertical angle 2β, which are—for symmetry reasons—half the viewing angles. They are related to (x,r) by:

$$\sin(2\alpha) = \frac{2x}{\sqrt{(x^2-(r-R)^2)(x^2+(r-R)^2)}} \quad \sin\beta = \frac{R}{\sqrt{x^2+r^2+R^2}} \tag{9}$$

Finally, following normalisation, the radial function becomes:

$$G(x,r) = \sin(\alpha)\sin(\beta)\frac{x^2}{x^2+R^2} \tag{10}$$

To capture the speed-up downwind of the rotor the induction is mirrored in the rotor plane and its sign swapped.

2.5. Vortex ring model

The vortex ring model is not implemented in PyWake, due to its high computational cost. Nevertheless, it is included in the comparison, as it explicitly models the expansion of the near wake, whereas all other previously presented analytical models neglect it. It achieves this by releasing vortex rings from the rotor, which freely expand under their self-induction. Only in the far wake where the expansion is halted is the wake represented again by a cylinder. A detailed description of the implementation is given in the Appendix of [1].

2.6. Rankine-half-body with wake expansion

The Rankine-half-body with wake expansion (RHBW) model was developed by Brian Gribben and Graham Hawkes of Frazer-Nash within the Carbon Trust's Offshore Wind Accelerator programme[1]. The details of the underlying algorithm are pending publication and potential implementation in PyWake, but some results from this model are included here for comparison. RHBW builds upon the initial potential flow proposed by Gribben and Hawkes [9] and extends the potential flow source/vortex analogy to represent the near wake expansion more fully (as is already present in the vortex ring model) in a simple analytical manner. Whereas the initial potential flow model considered a single flow potential source located at the rotor hub, RHBW allows the source position and strength to vary. These variables can be solved for by matching the mass flow in the annular region between 1D momentum theory streamtube and Rankine-half-body surface at the rotor and asymptotically downstream (i.e., after wake expansion). The model is essentially an analytical extension of the initial potential flow model and as a result is equally as rapid to compute.

3. RANS-AD simulations

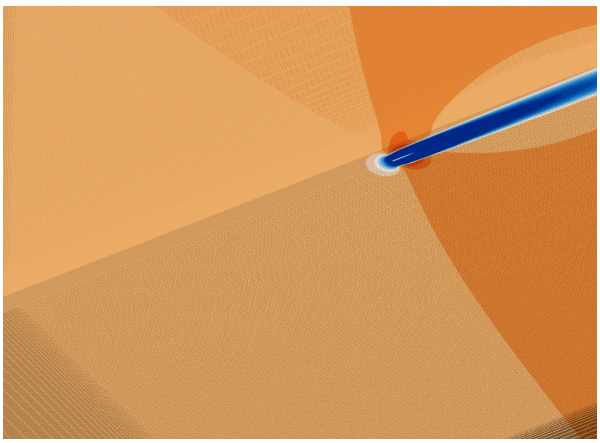

Figure 1. CFD simulation of an actuator disc showing the flow grid. Contours of streamwise velocity.

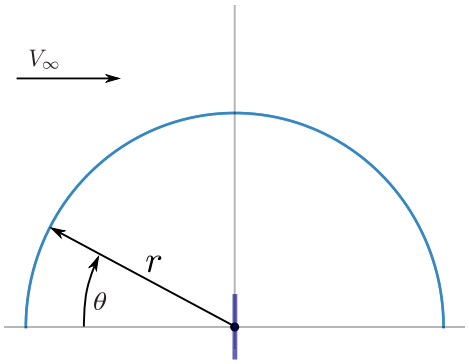

Figure 2. Schematic of flow data sampling in the horizontal plane at hub height around the turbine. The sampling path is indicated by a blue line.

[1] The Offshore Wind Accelerator (OWA) is a collaborative research, development and deployment programme with the aim to reduce the cost of offshore wind. The programme, run by the Carbon Trust, involves participation and funding from: EnBW, Equinor, Ørsted, RWE, Scottish Power Renewables, Shell, SSE Renewables, Total and Vattenfall Wind Power.

3.1. Numerical methodology

The simulations are performed within DTU Wind Energy's AEP tool PyWake using the CFD-RANS plug-in PyWakeEllipSys. This uses the DTU general purpose flow solver EllipSys3D [11, 12, 13], which solves the discretised incompressible Navier-Stokes equations. Here, the RANS equations are closed using the k-ω shear-stress transport model [14]. The actuator disc approach follows the implementation by Réthoré *et al.* [15], which uses an intersectional grid between polar AD and flow grid for distributing the forces. The polar disc grid is discretised by 64 radial and 32 azimuthal cells. Overall, the numerical setup follows that of Troldborg et al. [10], with the exception of the grid and domain.

Whereas previously the focus was on capturing the near-rotor behaviour of the induction zone, here we target investigating the far-field induction. Its magnitude is extremely sensitive to numerical errors and therefore the refined cubic mesh region is extensively extended with $94R$ x $94R$ x $6R$ side lengths, the latter representing the vertical extend. With the AD at its centre, the box domain has side lengths of $1000R$ to reduce any boundary-related errors. The refined mesh region is uniformly discretised by $R/8$, which is sufficient for an accurate representation of the rotor forces [16] (see figure 1). The grid has 144 million cells.

The velocity, pressure, and turbulence residuals are converged to at least 10^{-6}.

3.2. Simulation setup

The engineering models should induce velocities in the far field similar to existing wind turbines, yet simplify the blade loading to be constant across the rotor disc. The investigation by Troldborg and Meyer Forsting [10] found that a constantly loaded rotor induces velocities different from operating turbines upstream. Therefore—additionally to a constantly loaded rotor—here the DTU 10 MW and SWT 2.3 MW are simulated using 2D aerofoil data and following the specifications given in [10]. These turbines previously showed the lowest and greatest difference in induction, respectively, to the constantly loaded rotor.

From all simulations streamwise velocities are extracted in an arc around the turbine in the horizontal plane at hub height and at different radial stations, as shown in figure 2. The simulations are performed at constant wind speed, pitch, and rotational speed. The air density and dynamic viscosity are $\rho = 1.225$ kg/m^3 and $\mu = 1.784 \cdot 10^{-5}$ kg/m/s. As the rotors in the RANS simulations are simulated using aerofoil data, the rotor thrust coefficients are not known a priori. To allow for their intercomparison, results are interpolated if necessary. An example of the flow field developing around a turbine is shown in figure 1.

4. Results and Discussion

4.1. Model comparison

In figure 3, induced streamwise velocities predicted by analytical induction models and RANS-AD simulations are compared at different radial stations (rows) from the rotor and for two thrust coefficients (columns). Data points lie upstream for $\theta < 90°$ and downstream of the rotor plane for $\theta > 90°$. The focus here lies on the far-field behaviour, due to its importance in wind farm AEP simulations. The induced velocities near the rotor ($r/D = 1.0$) are only of interest when reference wind speed measurements upstream of a rotor are considered. Usually the induction of the mirror turbine—used for modelling the ground effect—for which the power is to be computed is not included, as its influence is already implicitly included in a turbine's power curve.

Generally, the magnitude of the induction decreases with distance from the rotor and diminishing thrust. All analytical models not accounting for wake expansion—only the vortex ring and RHBW model do—have the same shape, as the thrust coefficient simply acts as a scaling factor. At lower thrust levels (left column)—i.e., above rated wind speed—induction is independent of the turbine model; however around rated (right column), blade loading clearly

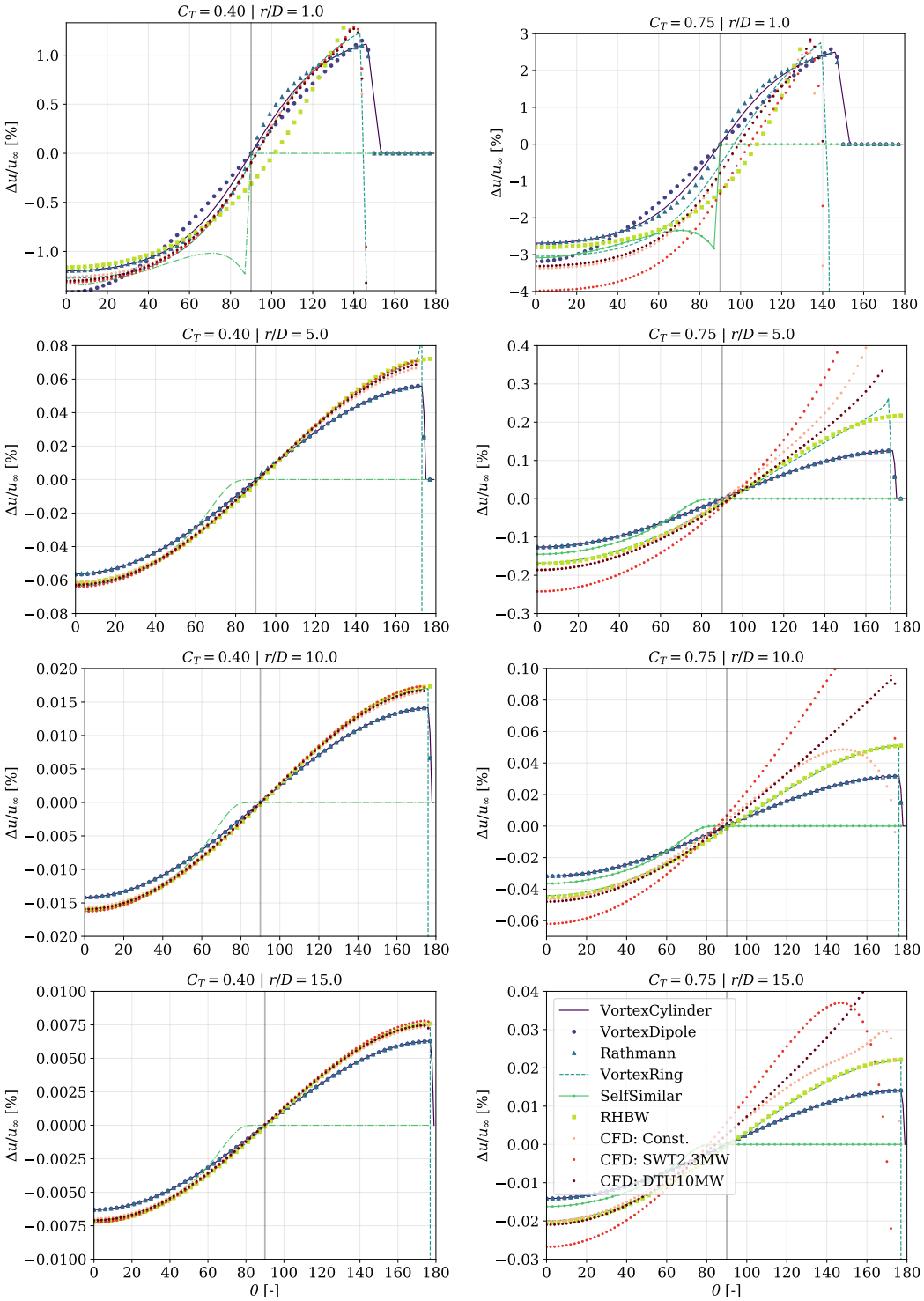

Figure 3. Comparison of induced streamwise velocities predicted by analytical induction models with RANS-AD simulations along different radial stations (rows) from the rotor and at two thrust coefficients (columns).

seems to play a role as the results for the SWT 2.3 MW show consistently more pronounced induction. This was also previously shown by Troldborg et al [10] and Meyer Forsting et al. [17], suggesting a correlation with blade loading/design. All vortex cylinder based models (VC, VD, VR) consistently underpredict induction independently of thrust, which also motivated Troldborg et al. in introducing a C_T scaling factor in the self-similar model. They also noted that it should probably not be a constant factor (which was chosen for simplicity), but increase with thrust as indicated by the consistent underprediction at higher thrust. As the self-similar model was intended for correcting lidar velocity measurements in the induction zone upstream and close to the rotor, it is only strictly valid in that region. The downstream flow acceleration is not captured but could be taken from another model. The analytical models including wake expansion—VR and RHBW—show consistently good agreement beyond $r/D \geq 2$ with the constantly loaded and DTU 10 MW CFD results. Closer to the rotor results diverge, which might be of little concern for wind farm simulations.

The CFD results show that the term "wind farm blockage" might be misleading, as downstream ($\theta > 90°$) the flow divergence caused by a rotor's blockage introduces speed-ups of equal magnitude to the deficits upstream. Instead of considering blockage solely as an energy sink, it should really be seen as an energy redistribution mechanism. Thus, when an engineering blockage model is included in fast AEP computations, the speed-ups also need to be modelled, otherwise there will be a bias toward lower AEP. For the vortex-cylinder-based models, the induction downstream is mirrored in the rotor plane and opposite in sign. Below rated this "mirroring" seems an adequate approximation, though the speed-up is actually minutely larger. RHBW and VR also agree downstream with the CFD results at below-rated thrust levels ($C_T < 0.5$); however at larger levels increasingly under-predict the speed-ups. Yet, the latter also shows significant turbine dependency and most likely rests on the wake breakdown mechanism. In turn, the breakdown depends on the ambient atmospheric conditions, most prominently inflow turbulence, which is not modelled in these CFD simulations. Once turbulence is introduced, it dominates wake breakdown and not turbine-specific blade loading.

For wind farm yield optimisation and uncertainty quantification, computational speed is of the essence, therefore requiring fast blockage models. The computational performance of the different models presented herein is compared in table 1. They are compared by expressing them relative to the fastest model (i.e., the self-similar one9. The vortex dipole, Rathmann, and RHBW models are of similar speed, whereas the vortex cylinder and ring are about two orders of magnitude more expensive. The cost of the CFD simulations is only given for reference. For fast AEP evaluations, thus only the fastest group of models should be considered.

4.2. Modified Rathmann

Following the attempt by Troldborg et al. [10] to scale the induction predicted by a vortex cylinder along the turbine centreline to achieve greater agreement between the self-similar model and the CFD simulations, an attempt is made to scale the Rathmann prediction accordingly. The idea is to create a fast and simple model that is sufficiently accurate in the region where $r/D \geq 1$. The scaled results furthermore help isolate the influence of wake expansion on induction.

In figure 4 the ratio between the streamwise-induced velocities predicted by the Rathmann model along the rotor centreline ($\theta = 0°$) is shown with respect to models including wake expansion as a function of thrust and along fixed radial positions from the rotor. The ratio generally increases with thrust, resulting from similarly increasing wake expansion. Interestingly, the curves start collapsing beyond $r/D > 5$. This is reminiscent of the classification of the wake into near and far regions. Beyond $r/D = 5$ from the rotor, the near-wake expansion has little influence, as from such a distance the wake seems fully expanded. Only coming closer to the rotor does it manifest itself.

Table 1. Computational performance comparison. The time per flow grid point is computed by dividing a model's total compute time by the total flow evaluation points and number of thrust levels. [1] Nonoptimized Matlab implementation. [2] Performed on another system; however, identical to VD speed. [3] Average performance for 144 million grid cells on 273 CPUs and at least 1000 iterations.

Model	Time per compute point [s]	Relative time [-]
Self similar	2.94 $\times 10^{-7}$	1.0
Vortex dipole	3.16 $\times 10^{-7}$	1.1
Rathmann	4.90 $\times 10^{-7}$	1.7
Vortex cylinder	3.54 $\times 10^{-5}$	64
Vortex ring[1]	5.46 $\times 10^{-5}$	186
RHBW[2]	-	1.1
CFD[3]	1.24 $\times 10^{-2}$	4.22 $\times 10^{3}$

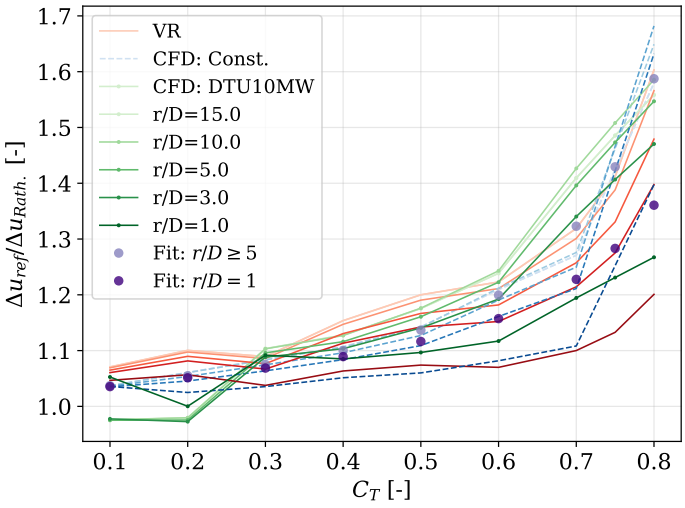

Figure 4. Ratio of the streamwise-induced velocities predicted by the Rathmann model to those by higher-fidelity models at different radial stations and its evolution with thrust coefficient for $\theta = 0$. The curve fit from equation (13) is given for reference.

A simple fit to the curves in figure 4 takes the form:

$$f = c_1 \exp(c_2 g C_T) + c_3 \exp(c_4 g C_T) \tag{11}$$

$$g^\star = 1 + c_5(r - 5) \tag{12}$$

$$g = \min(g^\star, 1.0) \quad \text{and} \quad g = \max(g^\star, 1 - 4c_5) \tag{13}$$

with model constants, $c = [1.02, 1.55 \times 10^{-1}, 5.01 \times 10^{-4}, 8.45, 2.50 \times 10^{-2}]$. This is only a possible fit that seems to approximate the CFD results satisfactorily, but other fits are of course equally valid. Figure 5 shows the beneficial impact of the re-scaled Rathmann results, but also highlights, as previously mentioned, that the magnitude of the induced velocities up and

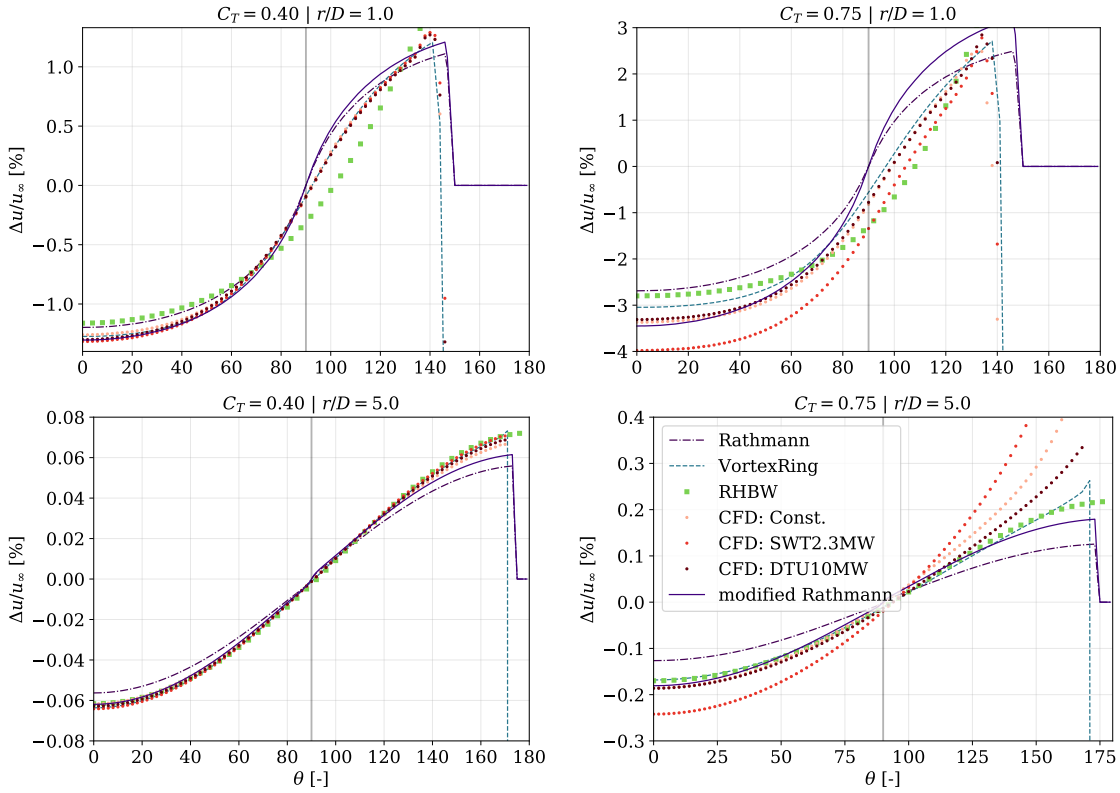

Figure 5. Comparison of the modified Rathmann model with respect to the simulations of higher fidelity.

downstream is not identical. Close to the rotor ($r/D = 1$), the modified Rathmann model now also shows good agreement upstream with respect to the CFD results. Although this is not true downstream, it has little practical significance.

4.3. Five laterally aligned turbine test case

Meyer Forsting et al. [1] previously investigated the power variation along a row of aligned wind turbine rotors caused by blockage effects alone (see figure 6). They showed a noticeable variation with respect to the inflow angle—the angle between the rotor alignment axis and wind direction of the incoming flow (defined as zero when perpendicular). A loss in production (with respect to an isolated rotor) was observed at the most upstream turbine that turned into a gain moving down the row. As this is a pure blockage-driven phenomenon, it serves as a great test case for evaluating the performance of the previously presented blockage models. The distance between the turbines is $3D$, there is no ground plane and the thrust across the row is fixed at $C_T = 0.798$, which is identical to the CFD setup. The induction from different rotors is simply summed, as it only presents a small perturbation to the mean flow.

As expected, the vortex-cylinder-type models (VC, VD, Rathmann) again fall on top of each other. Although the ground effect is not modelled here, results will not change as all these models yield nearly identical results from $r/D > 1$. The shape of the power variation for nonzero inflow angle are similar to those seen in the CFD simulations, indicating negative induction at the first and positive induction at the last turbine, but the magnitude is off. The VC models predict the power variation at 45° to be at the same levels as the CFD results with a 30° inflow angle.

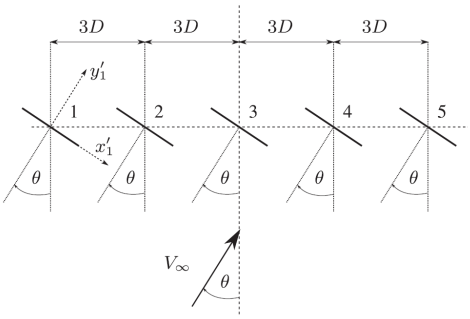

Figure 6. Row of five aligned turbines under varying inflow direction.

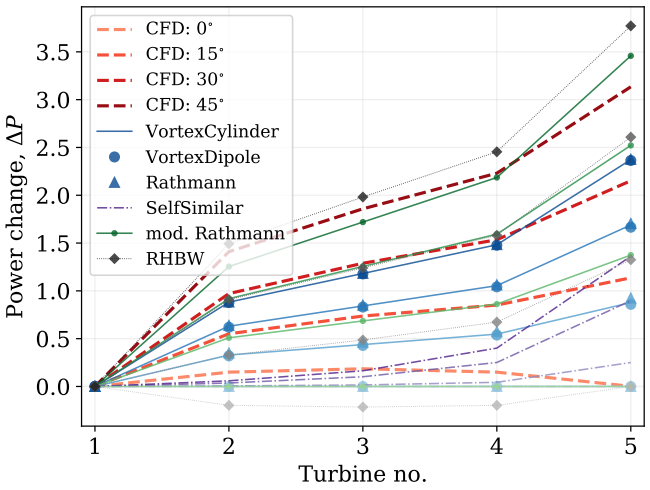

Figure 7. Change in power along a row of laterally aligned turbines with inflow direction, where Turbine 1 is the most upstream (refer to figure 6). CFD results from Meyer Forsting et al. [1]. The self-similar model is shown to indicate the consequence of missing blockage-related speed-ups.

The modified Rathmann and RHBW, on the other hand, predict power variations closest to the CFD results. The self-similar model is solely shown here to highlight the consequence of missing the blockage-related speed-ups in wind farm simulations.

A special condition occurs when the inflow is perpendicular to the row (0°). All models except the RHBW predict zero power variation. The reason for this lies in the RHBW inducing negative velocities in the rotor plane, which are due to wake expansion. Meyer Forsting et al. [1] noted the same behaviour for the vortex ring model, when the wind turbine wakes were uncoupled. Once coupled, the variation also vanished. Wake coupling was similarly identified by Meyer Forsting et al. to lead to a power gain toward the central turbine in the CFD simulations. Wake advection is accelerated for the inner turbines under the influence of the induced speed-ups from neighbouring rotors, leading to lower induction in the rotor plane.

5. Conclusion

With rising concerns over wind farm blockage, the interest in incorporating induction zone models into existing AEP estimators has grown. Yet, the proof of their validity in the far field region—most relevant in wind farm simulations—is missing. By comparing an extensive set of analytical induction zone models to RANS-AD simulations of different wind turbine models (including a constantly loaded disc, which is commonly employed by modellers), the following conclusions emerged:

(i) Blockage redistributes energy; unlike wakes, it should not be interpreted as pure energy sink. Generally it induces wind speed deficits upstream of the rotor plane, which are more than matched by downstream gains.

(ii) The gain downstream is not equal and opposite the losses upstream, but instead is slightly larger.

(iii) Above rated (low thrust coefficient) a turbine's induction field is not turbine model specific. Around rated (high thrust) it is, especially the speed-ups downstream of the rotor plane.

(iv) Vortex-cylinder-based models systematically underpredict induction; increasingly so with increasing thrust level. This is due to missing wake expansion, which grows with thrust.

(v) A new Rankine-half-body model with wake expansion (RHBW) predicts blockage-related velocity perturbations similar to RANS-AD simulations at the computational cost of the fastest blockage models available

(vi) Summing blockage related velocity perturbations in a wind farm seems adequate

Our findings indicate that total wind farm AEP is—if at all—only slightly affected by the summed effect of individual turbine blockage, but instead leads to enhanced spatial variation in power production throughout a wind farm. This is due to deficits upstream of a rotor being matched by at least equal speed-ups downstream. Thus, when including blockage models in engineering wind farm AEP estimators, it is imperative to also include the downstream effect from blockage to avoid incurring an unrealistic bias toward AEP loss. Here it is important to note that this is not contradicting claims that an interaction between a wind farm and the atmospheric boundary layer (ABL), as proposed by Allaerts et al [5] for instance, could cause blockage-related AEP losses; this could well be the case, but these losses should not appear in engineering wind farm models without any coupled ABL model.

Finally, it should be investigated whether the turbine-specific speed-ups observed at larger thrust levels persist even under more realistic turbulent, atmospheric inflow.

Acknowledgments

Thanks to all parties involved in the Carbon Trust's Offshore Wind Accelerator for the many fruitful discussions on wind farm blockage and the opportunity to share some of our findings publicly; specifically results from the RHBW model developed for the consortium. The Offshore Wind Accelerator (OWA) is a collaborative research, development and deployment programme with the aim to reduce the cost of offshore wind. The programme, run by the Carbon Trust, involves participation and funding from: EnBW, Equinor, Ørsted, RWE, Scottish Power Renewables, Shell, SSE Renewables, Total and Vattenfall Wind Power.

This work was authored in part by the National Renewable Energy Laboratory, operated by Alliance for Sustainable Energy, LLC, for the U.S. Department of Energy (DOE) under Contract No. DE-AC36-08GO28308. Funding provided by the U.S. Department of Energy Office of Energy Efficiency and Renewable Energy Wind Energy Technologies Office. The views expressed in the article do not necessarily represent the views of the DOE or the U.S. Government. The U.S. Government retains and the publisher, by accepting the article for publication, acknowledges that the U.S. Government retains a nonexclusive, paid-up, irrevocable, worldwide license to publish or reproduce the published form of this work, or allow others to do so, for U.S. Government purposes.

References

[1] Meyer Forsting A, Troldborg N and Gaunaa M 2017 *Wind Energy* **20** 63–77 ISSN 1095-4244
[2] Segalini A and Dahlberg J Å 2020 *Wind Energy* **23** 120–128 ISSN 10991824 URL `https://doi.org/10.1002/we.2413`
[3] Nygaard N G, Steen S T, Poulsen L and Pedersen J G 2020 *Journal of Physics: Conference Series* **1618**
[4] Bleeg J, Purcell M, Ruisi R and Traiger E 2018 *Energies* **11** ISSN 19961073
[5] Allaerts D and Meyers J 2017 *Journal of Fluid Mechanics* **814** 95–130
[6] Branlard E, Quon E, Meyer Forsting A, King J and Moriarty P 2020 Wind farm blockage effects: comparison of different engineering models vol 1618 (IOP Publishing) ISSN 1742-6596 tORQUE 2020 ; Conference date: 28-09-2020 Through 02-10-2020 URL `https://www.torque2020.org/`
[7] Branlard E and Meyer Forsting A 2020 *Wind Energy* **23** 2068–2086 ISSN 1095-4244

[8] Branlard E and Gaunaa M 2014 *Journal of Wind Energy*
[9] Gribben B J and Hawkes G S 2019 A potential flow model for wind turbine induction and wind farm blockage Tech. rep. Frazer-Nash Consultancy
[10] Troldborg N and Meyer Forsting A R *Wind Energy* n/a–n/a ISSN 1099-1824 we.2137 URL `http://dx.doi.org/10.1002/we.2137`
[11] Sørensen N 1995 *General purpose flow solver applied to flow over hills* Ph.D. thesis Risø National Laboratory
[12] Michelsen J 1994 Basis3d - a platform for development of multiblock pde solvers Tech. rep. Dept. of Fluid Mechanics, Technical University of Denmark, DTU
[13] Michelsen J 1994 Block structured multigrid solution of 2d and 3d elliptic pde's Tech. rep. Dept. of Fluid Mechanics, Technical University of Denmark, DTU
[14] Menter F R 1993 Zonal two equation $k-\omega$ turbulence models for aerodynamic flows 23^{rd} *Fluid Dynamics, Plasmadynamics, and Lasers Conference, Fluid Dynamics and Co-located Conferences* (Orlando,FL)
[15] Réthoré P E, van der Laan P, Troldborg N, Zahle F and Sørensen N 2014 *Wind Energy*
[16] van der Laan P, Sørensen N N, Réthoré P E, Mann J, Kelly M C, Troldborg N, Schepers J G and Machefaux E 2014 *Wind Energy*
[17] Meyer Forsting A, Troldborg N, Bechmann A and Réthoré P E 2017 *Modelling Wind Turbine Inflow: The Induction Zone* Ph.D. thesis DTU Wind Energy Denmark